

# Total Angular Momentum Coherent State Fields

D. Aguirre-Olivas,<sup>1,\*</sup> G. Mellado-Villaseñor,<sup>1,†</sup>

Benjamin Perez-Garcia,<sup>2,‡</sup> and B. M. Rodríguez-Lara<sup>3,§</sup>

<sup>1</sup>*Instituto Nacional de Astrofísica, Óptica y Electrónica,  
Tonantzintla, Puebla 72840, Mexico.*

<sup>2</sup>*Photonics and Mathematical Optics Group,  
Tecnologico de Monterrey, Monterrey 64849, Mexico.*

<sup>3</sup>*Universidad Politécnica Metropolitana de Hidalgo, Tolcayuca, Hidalgo 43860, Mexico.*

(Dated: March 6, 2026)

## Abstract

Structured light fields exploit spin and orbital angular momentum for precision manipulation, advanced imaging, and high-capacity communication. Orbital angular momentum coherent state beams interpolate between Hermite– and Laguerre–Gaussian beams, enabling continuous spatial control. We introduce a symmetry-based framework for joint control of polarization and spatial structure under the shared  $su(2)$  Lie algebra of spin and orbital angular momentum. Within this structure, we construct total angular momentum fields as superpositions of circular polarization and Laguerre–Gaussian beams, and define their  $su(2)$  coherent states within fixed-angular-momentum subspaces. A single complex parameter controls both polarization and spatial degrees of freedom, enabling continuous, symmetry-preserving tuning.

---

\* e-mail: dilia.aguirre@inaoe.mx

† e-mail: gmelladov@inaoe.mx

‡ e-mail: b.pegar@tec.mx

§ e-mail: blas.rodriguez@gmail.com

## I. INTRODUCTION

Optical fields carry two forms of angular momentum: spin angular momentum (SAM), associated with polarization [1], and orbital angular momentum (OAM), associated with phase structure [2–4]. SAM is intrinsic and independent of the reference axis [5], with left- and right-circular polarizations carrying  $\pm\hbar$  per photon [6], while linear polarization carries none. OAM may be intrinsic or extrinsic [7]. Laguerre–Gaussian beams (LGBs) carry intrinsic OAM  $\hbar\ell$  per photon with integer topological charge  $\ell$  [8]. Symmetric apodization preserves intrinsic OAM [9], while asymmetric induces extrinsic contributions [7]. Total angular momentum (TAM) combines both SAM and OAM.

Structured light fields exhibit spatially varying polarization, amplitude, and phase, carrying both SAM and OAM [10–13]. Polarization–spatial coupling arises naturally in them [14], enabling spin-dependent beam shifts [15], spin-to-orbit conversion [16], classical entanglement [17], and coupled intensity–angular momentum moments [18]. Geometric visualizations such as the Poincaré sphere [19–21] and Majorana constellation [22] capture these couplings. Structured fields generated using spiral phase plates [23],  $q$ - and  $j$ -plates [24, 25], metasurfaces [26], optically active materials [27], and phase-only modulators [28–30] enable independent or joint control over polarization, amplitude, and phase. Recent advances demonstrated cylindrical [11, 31, 32], helico-conical [33], and hybrid Hermite–Laguerre–Gaussian beams [34] with tailored angular momentum structure, as well as the generation, filtering, and processing of TAM eigenstates [35, 36], driving applications in optical trapping [37–39], high-resolution imaging [40, 41], and classical and quantum communication [42–48].

Here, we construct total angular momentum coherent state (TAMCS) fields, extending our recent orbital angular momentum coherent state (OAMCS) beams that interpolate between HGBs and LGBs [49]. Circular polarization and LGBs form orthonormal bases for SAM and OAM. From them, we build TAM fields as Clebsch–Gordan superpositions of spin and orbital components, identifying radial and azimuthal polarization modes within fixed-TAM subspaces. We then define TAMCS fields as  $su(2)$  coherent superpositions within each TAM subspace, where a single complex parameter jointly controls polarization and spatial structure.

## II. ORTHONORMAL LGBS

We construct our orthonormal basis for structured light fields as the product of polarization and spatial degrees of freedom (DoFs). For the polarization DoF, we use left- and right-circular states. For the spatial DoF, we use LGBs,

$$\Psi_{p,\ell}(r, \theta, z) = \frac{\sqrt{2}}{w(z)} e^{-\frac{ikr^2}{2R(z)}} e^{i(2p+|\ell|+1)\zeta(z)} \psi_{p,\ell}(\rho, \theta), \quad (1)$$

with beam width  $w(z) = w_0 \sqrt{1 + (z/z_R)^2}$ , curvature radius  $R(z) = z[1 + (z/z_R)^2]$ , and Gouy phase  $\zeta(z) = \tan^{-1}(z/z_R)$ . We use the waist radius  $w_0 = \sqrt{\lambda z_R/\pi}$ , Rayleigh range  $z_R = \pi w_0^2/\lambda$ , wavenumber  $k = 2\pi/\lambda$ , and wavelength  $\lambda$ . Each beam includes a transverse profile defined by the Laguerre–Gauss modes,

$$\psi_{p,\ell}(\rho, \phi) = (-1)^p \sqrt{\frac{p!}{\pi(p+|\ell|)!}} \rho^{|\ell|} e^{-\frac{1}{2}\rho^2} L_p^{|\ell|}(\rho^2) e^{i\ell\phi}, \quad (2)$$

with scaled radial coordinate  $\rho = \sqrt{2}r/w(z)$  and azimuthal angle  $\phi$ . The indices  $p$  and  $\ell$  define the number of radial and angular nodes, determining the amplitude and phase structure of each beam.

## III. TOTAL ANGULAR MOMENTUM LIGHT FIELDS

We construct light fields with well-defined TAM by coupling the polarization and spatial DoFs that carry SAM and OAM, respectively. We map circular polarization to the spin-1/2 basis  $|s, m_s\rangle$  with  $s = 1/2$  and  $m_s = \pm 1/2$ , identifying left-circular polarization with  $|1/2, 1/2\rangle$ . We map LGBs to the Dicke spin- $j$  basis  $|j, m_j\rangle$ , with  $j = (2p + |\ell|)/2 = 0, 1/2, 1, \dots$  and  $m_j = \ell/2$  [50]. This construction exploits the shared  $su(2)$  symmetry of SAM and OAM.

Combining  $s = 1/2$  and  $j = 0, 1/2, 1, \dots$  using  $su(2)$  addition rules produces two TAM subspaces with  $J = |s - j|$  and  $J = s + j$ , each spanned by  $2J + 1$  states labeled by  $M = -J, -J + 1, \dots, J - 1, J$ . Each TAM state is a SAM-OAM product basis superposition,

$$|J, M\rangle = \sum_{m_s = -\frac{1}{2}}^{\frac{1}{2}} \sum_{m_j = -j}^j c_{s, m_s; j, m_j}^{J, M} |s, m_s\rangle \otimes |j, m_j\rangle, \quad (3)$$

with weights given by the Clebsch–Gordan coefficients,

$$c_{s,m_s;j,m_j}^{J,M} = (-1)^{s-j+M} \sqrt{2J+1} \begin{pmatrix} s & j & J \\ m_s & m_j & -M \end{pmatrix}, \quad (4)$$

expressed via the Wigner  $3j$ -symbol and computed using the Racah formula [51]. These coefficients ensure  $M = m_s + m_j$  and enforce the triangle inequality  $|s - j| \leq J \leq s + j$  [52].

We define the optical realization of a TAM state as

$$E_{J,M}^{(j)}(\mathbf{r}) = \sum_{m_s=-\frac{1}{2}}^{\frac{1}{2}} \sum_{m_j=-j}^j c_{s,m_s;j,m_j}^{J,M} \epsilon_{m_s} \Psi_{j-|m_j|, 2m_j}(\mathbf{r}), \quad (5)$$

where  $\epsilon_{m_s} = \epsilon_{\pm 1/2}$  denote left- and right-circular polarization states. All LGBs in the superposition share the same total node number  $N = 2p + |\ell| = 2j$ , so they experience identical curvature phase, Gouy phase, and beam scaling. As a result, our TAM light fields preserve their transverse polarization and spatial structure under paraxial propagation up to a scaling factor.

As an example,  $j = 1/2$  produces a singlet with  $J = 0$  and a triplet with  $J = 1$ . The singlet state with  $M = 0$  is

$$E_{0,0}^{(\frac{1}{2})}(\mathbf{r}) = \sqrt{\frac{1}{2}} \left[ \epsilon_{-\frac{1}{2}} \Psi_{0,1}(\mathbf{r}) - \epsilon_{\frac{1}{2}} \Psi_{0,-1}(\mathbf{r}) \right], \quad (6)$$

with azimuthal polarization, Fig. 1(a). The triplet states with  $M = -1, 0, 1$  are

$$\begin{aligned} E_{1,-1}^{(\frac{1}{2})}(\mathbf{r}) &= \epsilon_{-\frac{1}{2}} \Psi_{0,-1}(\mathbf{r}), \\ E_{1,0}^{(\frac{1}{2})}(\mathbf{r}) &= \sqrt{\frac{1}{2}} \left[ \epsilon_{-\frac{1}{2}} \Psi_{0,1}(\mathbf{r}) + \epsilon_{\frac{1}{2}} \Psi_{0,-1}(\mathbf{r}) \right], \\ E_{1,1}^{(\frac{1}{2})}(\mathbf{r}) &= \epsilon_{\frac{1}{2}} \Psi_{0,1}(\mathbf{r}), \end{aligned} \quad (7)$$

exhibiting right-circular, radial, and left-circular polarization, respectively, Fig. 1(b)–(d).

#### IV. AZIMUTHAL AND RADIAL POLARIZATION

We extend our construction to higher-order OAM components  $j = 3/2, 5/2, 7/2, \dots$ , which yield two integer-TAM subspaces with  $J = |1/2 \pm j|$ . The corresponding  $M = 0$  states,

$$\begin{aligned} E_{j-\frac{1}{2},0}^{(j)}(\mathbf{r}) &= \frac{1}{2} \left[ \epsilon_{-\frac{1}{2}} \Psi_{j-\frac{1}{2},1}(\mathbf{r}) - \epsilon_{\frac{1}{2}} \Psi_{j-\frac{1}{2},-1}(\mathbf{r}) \right], \\ E_{j+\frac{1}{2},0}^{(j)}(\mathbf{r}) &= \frac{1}{2} \left[ \epsilon_{-\frac{1}{2}} \Psi_{j-\frac{1}{2},1}(\mathbf{r}) + \epsilon_{\frac{1}{2}} \Psi_{j-\frac{1}{2},-1}(\mathbf{r}) \right], \end{aligned} \quad (8)$$

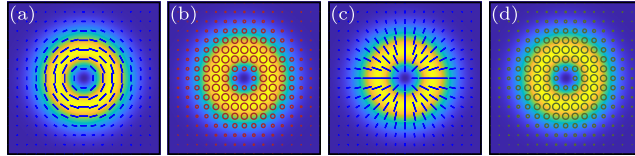


FIG. 1. Intensity and polarization distributions for TAM states with  $j = 1/2$ . (a) Singlet state with  $\{J, M\} = \{0, 0\}$ . (b)-(d) Triplet states with  $J = 1, M = -1, 0, 1$ . Vector field colors indicate linear (blue), right- (brown), and left-handed (green) polarizations.

yield azimuthal and radial polarization, respectively,

$$\begin{aligned}\epsilon_{-\frac{1}{2}}e^{i\theta} - \epsilon_{\frac{1}{2}}e^{-i\theta} &= -2i\epsilon_{\theta}, \\ \epsilon_{-\frac{1}{2}}e^{i\theta} + \epsilon_{\frac{1}{2}}e^{-i\theta} &= 2\epsilon_r,\end{aligned}\tag{9}$$

where  $\epsilon_{\theta} = -\epsilon_x \sin \theta + \epsilon_y \cos \theta$  and  $\epsilon_r = \epsilon_x \cos \theta + \epsilon_y \sin \theta$  are unit vectors for linear polarization in the azimuthal and radial directions, respectively. Each field pair defines orthonormal polarization states with identical intensity distributions  $|\Psi_{j-1, \pm 1}(\mathbf{r})|^2$ . Figure 2(a) and Fig. 2(b) show fields with azimuthal and radial polarization, respectively, for  $\{J, M\} = \{j \pm 1/2, 0\}$  with  $j \in \{3/2, 5/2, 7/2\}$ .

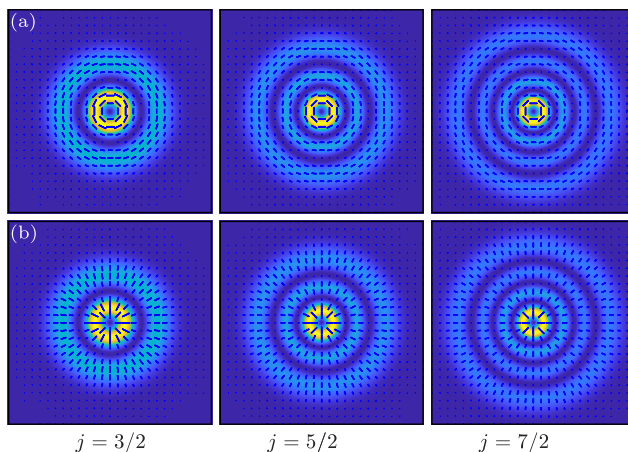


FIG. 2. Intensity and polarization distributions for (a) azimuthally and (b) radially polarized TAM fields for  $\{J, M\} = \{j \pm 1/2, 0\}$  with  $j \in \{3/2, 5/2, 7/2\}$ . Vector field colors follow Fig. 1.

## V. TAMCS

We previously introduced OAMCS beams that interpolate between HGBs and LGBs, using their  $su(2)$  symmetry [49]. Here, we introduce light field analogues to TAMCS,

$$E_{J,M,\alpha}^{(j)}(\mathbf{r}) = \sum_{q=-J}^J c_q(J, M, \alpha) E_{J,q}^j(\mathbf{r}), \quad (10)$$

where  $\alpha = |\alpha|e^{i\varphi}$  is a complex parameter enabling continuous joint control over polarization and spatial DoFs through the weights,

$$\begin{aligned} c_q(J, M, \alpha) = & \sqrt{\binom{2J}{J+q} \binom{2J}{J-M}} \times \\ & \times {}_2F_1(-J-q, -J+M; -2J; \csc^2 |\alpha|) \times \\ & \times e^{i\varphi(-M-q)} (\sec |\alpha|)^{-2J} (\tan |\alpha|)^{2J-M+q}, \end{aligned} \quad (11)$$

derived from the optical spatial-mode analogues of quantum coherent states [22, 50, 53]. We use the binomial coefficient  $\binom{a}{b} = a!/[b!(a-b)!]$  and the Gauss hypergeometric function  ${}_2F_1(a, b; c; z)$ . All fields in the superposition belong to the same TAM subspace with modal number  $N = j$ , so TAMCS fields retain their transverse structure under paraxial propagation up to a scale factor.

We use TAMCS fields with  $\{J, M\} = \{1, 0\}$  to illustrate how the amplitude  $|\alpha|$  modulates polarization and spatial structure with  $\pi$ -periodicity. Figures 3(a) and 3(b) show the weight magnitudes  $|c_q|$  for  $j = 1/2$  and  $j = 3/2$  at fixed phase  $\varphi = 0$  and amplitudes  $|\alpha| \in \{0, \pi/8, \pi/4\}$ , at  $z = 0$ . We show the corresponding intensity and polarization distributions in Figs. 3(c)–(d).

For fixed amplitude  $|\alpha|$ , varying the coherent parameter phase  $\varphi$  rotates both polarization and spatial structure by  $\varphi/2$  around the optical axis with  $2\pi$ -periodicity. Figure 4(a) shows this effect for  $|\alpha| = \pi/8$  and phases  $\varphi \in \{0, \pi/4, \pi/2\}$ , at  $z = 0$ . To characterize polarization, we use the space-resolved Stokes parameters [54],

$$\begin{aligned} S_0(\mathbf{r}) &= |E_+(\mathbf{r})|^2 + |E_-(\mathbf{r})|^2, \\ S_1(\mathbf{r}) &= 2\text{Re}[E_-(\mathbf{r})^* E_+(\mathbf{r})], \\ S_2(\mathbf{r}) &= -2\text{Im}[E_-(\mathbf{r})^* E_+(\mathbf{r})], \\ S_3(\mathbf{r}) &= |E_-(\mathbf{r})|^2 - |E_+(\mathbf{r})|^2, \end{aligned} \quad (12)$$

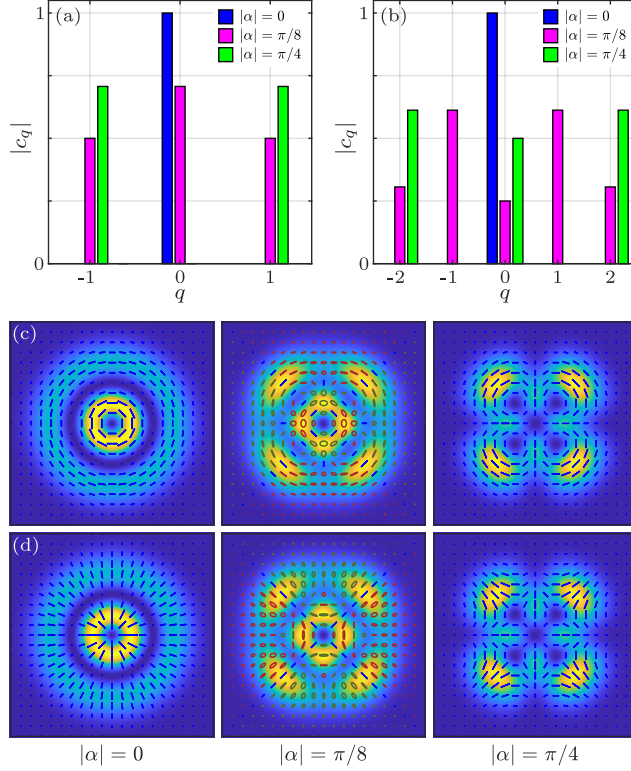


FIG. 3. (a)-(b) Weight magnitudes  $|c_q|$ , (c)-(d) intensity and polarization distribution for TAMCS fields with  $\{J, M\} = \{1, 0\}$  with (a),(c)  $j = 1/2$  and (b),(d)  $j = 3/2$  for  $\varphi = 0$  and  $|\alpha| \in \{0, \pi/8, \pi/4\}$ . Vector field colors follow Fig. 1.

in terms of the circular polarization components  $E_{\pm}(\mathbf{r})$ . From these, we recover the local polarization ellipse parameters,

$$A_{\pm}(\mathbf{r}) = \left[ \frac{S_0(\mathbf{r}) \pm \sqrt{S_1^2(\mathbf{r}) + S_2^2(\mathbf{r})}}{2} \right]^{1/2}, \quad (13)$$

$$\chi(\mathbf{r}) = \frac{1}{2} \arctan \left[ \frac{S_2(\mathbf{r})}{S_1(\mathbf{r})} \right], \quad (14)$$

where  $A_{\pm}$  are the semi-axes and  $\chi$  is the orientation angle. We map the resulting polarization states for the previous example onto the Poincaré sphere in Fig. 4(b). The polarization distribution on the Poincaré sphere exhibits rigid rotation by an angle  $\varphi/2$  around the  $S_3$  axis.

In Figure 5, we illustrate the vectorial nature of the TAMCS field for the parameter set  $\{J, M, j\} = \{1, 0, 3/2\}$ ,  $|\alpha| = \pi/4$ , and  $\varphi = \pi/2$ . The theoretical and experimental results for this configuration are presented in the upper and lower rows, respectively. The intensity distributions correspond to (a) the TAMCS field and to the field transmitted through a linear

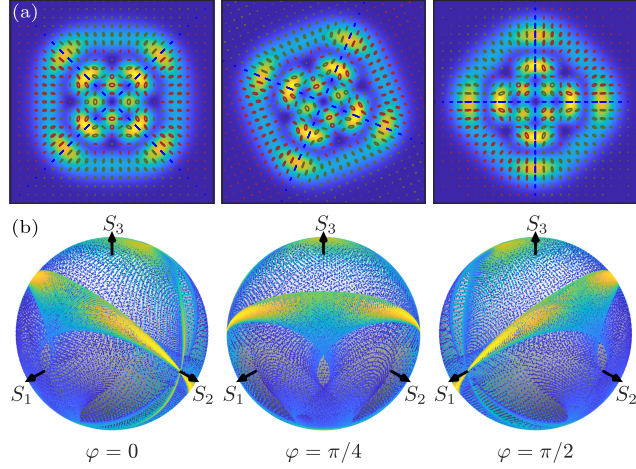


FIG. 4. (a) Intensity and polarization distribution, and (b) polarization mapped on the Poincaré sphere for TAMCS fields with  $\{J, M, j\} = \{3, 0, 5/2\}$ ,  $|\alpha| = \pi/8$ , and  $\varphi \in \{0, \pi/4, \pi/2\}$ . Vector field colors follow Fig. 1

polarizer whose transmission axis is set to (b)  $0^\circ$ , (c)  $45^\circ$ , and (d)  $90^\circ$ , where the angles are referenced to the horizontal axis. The experimental results were obtained following the procedure describe in [29], showing good agreement with the corresponding theoretical simulations.

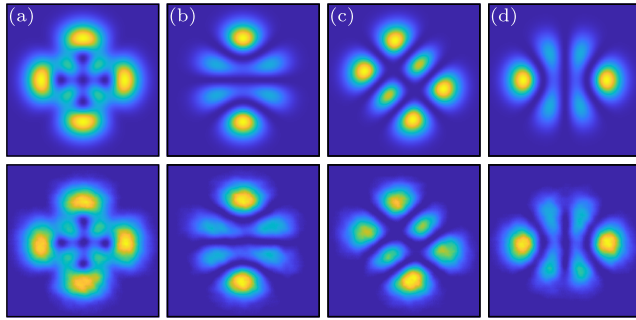


FIG. 5. Theoretical (upper line) and experimental (lower line) results of a TAMCS field with parameters  $\{J, M, j\} = \{1, 0, 3/2\}$ ,  $|\alpha| = \pi/4$ , and  $\varphi = \pi/2$ . Intensity distributions of (a) the TAMCS field and after transmission through a linear polarizer with its transmission axis oriented at (b)  $0^\circ$ , (c)  $45^\circ$ , and (d)  $90^\circ$ , with respect to the horizontal.

## VI. CONCLUSION

In summary, we built an orthonormal basis for structured light fields by pairing circular polarization and LGBs, mapped to spin-1/2 and spin- $j$  representations of SAM and OAM, respectively.

We constructed TAM fields as Clebsch–Gordan superpositions of this basis, generating complete subspaces with fixed TAM  $J = |1/2 \pm j|$  and projection  $M = -J, \dots, J$ . For  $j = 1/2, 3/2, 5/2, \dots$ , the  $M = 0$  states yield orthonormal light field pairs with radial and azimuthal polarization and identical intensity profile  $|\Psi_{j-1/2, \pm 1}(\mathbf{r})|^2$ .

We then introduced TAMCS as  $su(2)$  coherent superpositions within each  $J$  subspace, governed by a single complex parameter  $\alpha = |\alpha|e^{i\varphi}$ . The amplitude  $|\alpha|$  modulates polarization and spatial structure with  $\pi$ -periodicity, while the phase  $\varphi$  induces a rigid rotation around the optical axis with  $2\pi$ -periodicity. These fields preserve both polarization and intensity distributions under paraxial propagation up to a scaling factor.

Our framework enables continuous, symmetry-preserving control of polarization and spatial DoFs through a single complex parameter under  $su(2)$  angular momentum symmetry.

## FUNDING

Not Applicable.

## ACKNOWLEDGMENTS

B. M. R. L. acknowledges support and hospitality as an affiliate visiting colleague at the Department of Physics and Astronomy, University of New Mexico. G. M. V. acknowledges SECIHTI Mexico for the postdoctoral grant. The authors acknowledge José Miguel Arroyo Hernández from CIT - Optical Workshop (INAOE) for the fabrication of the custom lenses used in this work.

## DISCLOSURES

The authors declare no conflicts of interest.

## DATA AVAILABILITY STATEMENT

All the data is available from the corresponding author upon reasonable request.

---

- [1] R. A. Beth, Mechanical detection and measurement of the angular momentum of light, *Phys. Rev.* **50**, 115 (1936).
- [2] L. Allen, M. W. Beijersbergen, R. J. C. Spreeuw, and J. P. Woerdman, Orbital angular momentum of light and the transformation of Laguerre-Gaussian laser modes, *Phys. Rev. A* **45**, 8185 (1992).
- [3] S. M. Barnett and L. Allen, Orbital angular momentum and nonparaxial light beams, *Optics Communications* **110**, 670 (1994).
- [4] S. Franke-Arnold, L. Allen, and M. Padgett, Advances in optical angular momentum, *Laser & Photonics Reviews* **2**, 299 (2008), <https://onlinelibrary.wiley.com/doi/pdf/10.1002/lpor.200810007>.
- [5] D. L. Andrews and M. Babiker, *The Angular Momentum of Light* (Cambridge University Press, 2013).
- [6] P. Das, L.-P. Yang, and Z. Jacob, What are the quantum commutation relations for the total angular momentum of light? Tutorial, *J. Opt. Soc. Am. B* **41**, 1764 (2024).
- [7] A. T. O’Neil, I. MacVicar, L. Allen, and M. J. Padgett, Intrinsic and extrinsic nature of the orbital angular momentum of a light beam, *Phys. Rev. Lett.* **88**, 053601 (2002).
- [8] L. Allen, M. Padgett, and M. Babiker, IV The orbital angular momentum of light, in *Progress in Optics XXXIX*, Vol. 39, edited by E. Wolf (Elsevier, 1999) pp. 291–372.
- [9] M. V. Berry, Paraxial beams of spinning light, in *Proc. SPIE*, Vol. 3487 (1998) p. International Conference on Singular Optics.
- [10] A. M. Yao and M. J. Padgett, Orbital angular momentum: origins, behavior and applications, *Adv. Opt. Photon.* **3**, 161 (2011).
- [11] Q. Zhan, Cylindrical vector beams: from mathematical concepts to applications, *Adv. Opt. Photon.* **1**, 1 (2009).
- [12] M. J. Padgett, Orbital angular momentum 25 years on [invited], *Opt. Express* **25**, 11265 (2017).

- [13] C. Rosales-Guzmán, B. Ndagano, and A. Forbes, A review of complex vector light fields and their applications, *J. Opt.* **20**, 123001 (2018).
- [14] K. Volke-Sepúlveda and E. Ley-Koo, General construction and connections of vector propagation invariant optical fields: TE and TM modes and polarization states, *J. Opt. A: Pure Appl. Opt.* **8**, 867 (2006).
- [15] K. Y. Bliokh and F. Nori, Transverse and longitudinal angular momenta of light, *Phys. Rep.* **592**, 1 (2015).
- [16] K. Y. Bliokh, F. J. Rodríguez-Fortuño, F. Nori, and A. V. Zayats, Spin-orbit interactions of light, *Nature Photonics* **9**, 796 (2015).
- [17] E. Karimi and R. W. Boyd, Classical entanglement?, *Science* **350**, 1172 (2015).
- [18] A. V. Volyar, E. G. Abramochkin, and M. V. Bretsko, Intertwining intensity moments and orbital angular momenta via astigmatic transforms of structured beams, *Opt. Mem. Neural Networks* **33**, S114 (2024).
- [19] D. Naidoo, F. S. Roux, A. Dudley, I. Litvin, B. Piccirillo, L. Marrucci, and A. Forbes, Controlled generation of higher-order Poincaré sphere beams from a laser, *Nat. Photon.* **10**, 327 (2016).
- [20] S. Fu, L. Hai, R. Song, C. Gao, and X. Zhang, Representation of total angular momentum states of beams through a four-parameter notation, *New J. Phys.* **23**, 083015 (2021).
- [21] W. Yu, H. Pi, M. Taylor, and J. Yan, Geometric representation of vector vortex beams: The total angular momentum-conserving Poincaré sphere and its braid clusters, *Photonics* **10**, 1276 (2023).
- [22] F. Torres-Leal, E. G. Herrera, M. P. Morales Rodríguez, B. Perez-Garcia, and B. M. Rodríguez-Lara, Majorana constellations for optical scalar beams and vector fields, *Phys. Rev. A* **110**, 063716 (2024).
- [23] M. Beijersbergen, R. Coerwinkel, M. Kristensen, and J. Woerdman, Helical-wavefront laser beams produced with a spiral phaseplate, *Optics Communications* **112**, 321 (1994).
- [24] L. Marrucci, C. Manzo, and D. Paparo, Optical spin-to-orbital angular momentum conversion, *Phys. Rev. Lett.* **96**, 163905 (2006).
- [25] R. C. Devlin, A. Ambrosio, N. A. Rubin, J. P. B. Mueller, and F. Capasso, Arbitrary spin-to-orbital angular momentum conversion of light, *Science* **358**, 896 (2017).

- [26] A. H. Dorrah, N. A. Rubin, M. Tamagnone, A. Zaidi, and F. Capasso, Structuring total angular momentum of light along the propagation direction with polarization-controlled meta-optics, *Nat. Commun.* **12**, 6249 (2021).
- [27] A. Karmakar and M. M. Brundavanam, Controlled generation of cylindrical vector vortex beams using an optically active material, *Opt. Lett.* **49**, 6145 (2024).
- [28] G. Mellado-Villaseñor, D. Aguirre-Olivas, U. Ruiz, and V. Arrizon, Generation of vector bessel beams with diffractive phase elements based on the jacobi-anger expansion, *J. Opt. Soc. Am. A* **35**, 28 (2018).
- [29] G. Mellado-Villaseñor, D. Aguirre-Olivas, and V. Arrizón, Generation of vector beams using synthetic phase holograms, *J. Opt. Soc. Am. A* **38**, 1094 (2021).
- [30] I. Moreno, J. A. Davis, M. M. Sánchez-López, and D. M. Cottrell, Shaped vector beams generated with a phase-only modulation—retarder optical configuration, *Opt. Lett.* **50**, 2298 (2025).
- [31] R. Chen, K. Mizutani, Y. Kozawa, and S. Sato, Generation of arbitrary cylindrical vector beams on the higher order Poincaré sphere, *Opt. Lett.* **39**, 5274 (2014).
- [32] S. N. Khonina, A. V. Ustinov, S. A. Fomchenkov, and A. P. Porfirev, Formation of hybrid higher-order cylindrical vector beams using binary multi-sector phase plates, *Sci. Rep.* **8**, 14320 (2018).
- [33] E. Medina-Segura, L. Miranda-Culin, V. Rodríguez-Fajardo, B. Perez-Garcia, and C. Rosales-Guzmán, Helico-conical vector beams, *Opt. Lett.* **48**, 4897 (2023).
- [34] E. Medina-Segura, L. Miranda-Culin, B. Perez-Garcia, C. Rosales-Guzmán, and M. A. Cox, Hybrid Hermite–Laguerre–Gaussian vector modes, *Opt. Lett.* **50**, 678 (2025).
- [35] Y. Shen, X. Wang, Z. Xie, C. Min, X. Fu, Q. Liu, M. Gong, and X. Yuan, Optical vortices 30 years on: Oam manipulation from topological charge to multiple singularities, *Light Sci. Appl.* **8**, 90 (2019).
- [36] L. Li, Y. Guo, Z. Zhang, Z. Shang, C. Li, J. Wang, L. Gao, L. Hai, C. Gao, and S. Fu, Photon total angular momentum manipulation, *Adv. Photonics* **5**, 056002 (2023).
- [37] M. J. Padgett and R. W. Bowman, Tweezers with a twist, *Nat. Photon.* **5**, 343 (2011).
- [38] H. Moradi, V. Shahabadi, E. Madadi, E. Karimi, and F. Hajizadeh, Efficient optical trapping with cylindrical vector beams, *Opt. Express* **27**, 7266 (2019).

- [39] E. A. Guzmán and A. V. Arzola, Enhancing near-field optical tweezers by spin-to-orbital angular momentum conversion, *J. Opt. Soc. Am. B* **39**, 1233 (2022).
- [40] A. F. Abouraddy and K. C. Toussaint, Three-dimensional polarization control in microscopy, *Phys. Rev. Lett.* **96**, 153901 (2006).
- [41] G. Bautista, J.-P. Kakko, V. Dhaka, X. Zang, L. Karvonen, H. Jiang, E. Kauppinen, H. Lipsanen, and M. Kauranen, Nonlinear microscopy using cylindrical vector beams: Applications to three-dimensional imaging of nanostructures, *Opt. Express* **25**, 12463 (2017).
- [42] E. Nagali and F. Sciarrino, Generation of hybrid polarization–orbital angular momentum entangled states, *Opt. Express* **18**, 18243 (2010).
- [43] N. Bozinovic, Y. Yue, Y. Ren, M. Tur, P. Kristensen, H. Huang, A. E. Willner, and S. Ramachandran, Terabit-scale orbital angular momentum mode division multiplexing in fibers, *Science* **340**, 1545 (2013).
- [44] A. E. Willner, H. Huang, Y. Yan, Y. Ren, N. Ahmed, G. Xie, C. Bao, L. Li, Y. Cao, Z. Zhao, J. Wang, M. P. J. Lavery, M. J. Padgett, S. J. Dolinar, and M. Tur, Optical communications using orbital angular momentum beams, *Adv. Opt. Photon.* **7**, 66 (2015).
- [45] G. Milione, T. A. Nguyen, J. Leach, D. A. Nolan, and R. R. Alfano, Using the nonseparability of vector beams to encode information for optical communication, *Opt. Lett.* **40**, 4887 (2015).
- [46] B. Ndagano, I. Nape, M. A. Cox, C. Rosales-Guzman, and A. Forbes, Creation and detection of vector vortex modes for classical and quantum communication, *Journal of Lightwave Technology* **36**, 292 (2018).
- [47] G. Ruffato, P. Capaldo, M. Massari, E. Mafakheri, and F. Romanato, Total angular momentum sorting in the telecom infrared with silicon Pancharatnam–Berry transformation optics, *Opt. Express* **27**, 15750 (2019).
- [48] Z. Zhu, M. Janasik, A. Fyffe, D. Hay, Y. Zhou, B. Kantor, T. Winder, R. W. Boyd, G. Leuchs, and Z. Shi, Compensation-free high-dimensional free-space optical communication using turbulence-resilient vector beams, *Nature Communications* **12**, 1666 (2021).
- [49] D. Aguirre-Olivas, G. Mellado-Villaseñor, B. Perez-Garcia, and B. M. Rodríguez-Lara, Orbital angular momentum coherent state beams, *Opt. Lett.* **50**, 1121 (2025).
- [50] M. P. Morales Rodríguez, E. García Herrera, O. S. Magaña-Loaiza, B. Perez-Garcia, F. Marroquín Gutiérrez, and B. M. Rodríguez-Lara, Spatial light mode analogues of generalized quantum coherent states, *Phys. Rev. A* **110**, 033523 (2024).

- [51] K. Kraus, Wigner3j symbol, <https://la.mathworks.com/matlabcentral/fileexchange/20619-wigner3j-symbol> (2008), [Online; accessed 27-January-2025].
- [52] D. A. Varshalovich, A. N. Moskalev, and V. K. Khersonskii, *Quantum Theory of Angular Momentum* (World Scientific, 1998).
- [53] M. P. Morales Rodríguez, O. S. Magaña-Loaiza, B. Perez-Garcia, L. M. Nieto, F. Marroquín Gutiérrez, and B. M. Rodríguez-Lara, Coherent states of Laguerre-Gauss modes, *Opt. Lett.* **49**, 1489 (2024).
- [54] D. H. Goldstein, *Polarized Light* (CRC Press, Boca Raton, 2011).